

Article

Effect of Chlorine-Containing VOCs on Silver Migration and Sintering in ZSM-5 Used in a TSA Process

Arnaud Monpezat ¹, Gabriel Couchaux ¹, Vincent Thomas ¹, Antoine Artheix ¹, Ludovic Deliere ¹, Claire Gréau ¹, Sylvain Topin ^{1,*}, Benoit Coasne ², Lucian Roiban ³, Luis Cardenas ⁴ and David Farrusseng ^{4,*}

¹ Commissariat à l’Energie Atomique et aux Energies Alternatives (CEA), DAM, DIF, F-91297 Arpajon CEDEX, France

² LIPhy, Université Grenoble Alpes, UMR 5588 CNRS, 38058 Grenoble CEDEX 9, 140 rue de la physique, France

³ MATEIS, University Lyon, INSA-Lyon, Université Claude Bernard Lyon I, UMR5510 CNRS, F-69621 Villeurbanne CEDEX, France

⁴ IRCELYON, University Lyon, Université Claude Bernard Lyon I, UMR 5256 CNRS, F-69626 Villeurbanne CEDEX, France

* Correspondence: sylvain.topin@cea.fr (S.T.); david.farrusseng@ircelyon.univ-lyon1.fr (D.F.); Tel.: +33-169-265-452 (S.T.); +33-472-445-365 (D.F.)

Received: 25 July 2019; Accepted: 10 August 2019; Published: 14 August 2019



Abstract: Silver nanoparticles are currently one of the most studied nanostructured nanomaterials. Because nanoparticle size and dispersion act together in determining a material’s physical and chemical properties, there is a continuous quest to develop size-controlled synthesis methods. Nonetheless, the instability of the nanometer-sized particles, which is caused by their tendency to aggregate irreversibly into larger particles, remains a recurrent problem. The use of confining scaffolds, such as the regular system of cages in a crystalline zeolite-type material, is often reported in the literature as an efficient solution to overcome particle migration at the surface. Silver nanoparticles encapsulated in ZSM-5 (Ag@ZSM-5) represent a new generation of adsorbent for Xe enrichment from the atmosphere that is currently being developed at the pilot scale in a Temperature Swing Adsorption (TSA) process. In this study, we have found that the presence of Cl-containing compounds in the air (VOCs) leads to a poisoning of the active silver phase by the formation of silver chloride. By a careful study of process parameters, we have found that most of the chlorine can be removed by heat treatment above 573 K so that the adsorption properties of silver are regenerated. That said, when applying 573 K temperature regeneration at the pilot scale, we observe a very minor but observable decay of xenon adsorption capacity that continues cycle after cycle. The mechanism of capacity decay is discussed in terms of (i) the residual presence of Cl at the surface of silver nanoparticles, (ii) the aggregation of silver nanoparticles into larger particles (sintering mechanism), and (iii) the acceleration of silver particle migration to the surface and sintering.

Keywords: zeolite; silver nanoparticles; sintering; poisoning; adsorption

1. Introduction

Among the noble gases, xenon is of the utmost economic importance, with numerous applications such as energy-efficient lightning [1], medicine [2], and chemical analysis [3]. Xenon radioisotopes are also used to monitor worldwide nuclear activities [4–7]. Nonetheless, the production cost of xenon (\$25/L according to Airgas® pricing in March 2013 for 99.995% research grade Xe) [8] and its very low

concentration in the air (87 ppbv) both contribute to limiting its use [9]. Xenon and krypton, which are produced industrially as byproducts of oxygen after cryogenic distillation, are enriched using adsorption processes and then separated by cryogenic distillation [10]. The development of alternative enrichment and separation processes that are more cost-efficient should facilitate the use of xenon by decreasing its price and allowing the expansion of its market. On the other hand, the enrichment and separation of Xe and Kr is also relevant for radioactivity release monitoring. In this context, the CEA in France has developed the SPALAX process [6,7,11] (Système de Prélèvement Automatique en Ligne avec l'Analyse du Xénon), which concentrates and purifies xenon from air samples prior to analytical measurement. In the concentration and separation process, permeation membranes are first used to eliminate H₂O, O₂, and CO₂. Then a Xe/Kr/N₂ separation is carried out in columns filled with active carbons in a Temperature Swing Adsorption (TSA) process, resulting in a xenon-enriched fraction.

Inspired by original works of Munakata et al. [12] and Kuznicki et al. [13] dealing with noble gas separation, we have investigated and developed silver-loaded zeolite for selective Xe/Kr/N₂ separation with the aim to replace the current technology based on active carbons, which exhibits only moderate capacity and selectivity. Among various zeolites, we have reported that highly-loaded silver faujasite and ZSM-5 (Ag@ZSM-5) are very efficient adsorbents for xenon at the ppm level [14,15]. At the pilot scale in relevant process conditions, we found that silver nanoparticles of 1–3 nm diameter in ZSM-5 zeolite at 9 wt.% loading show a 43-fold increase in capacity and a 45-fold increase in selectivity for Xe/Kr separation [15,16] with respect to the active carbon adsorbent used commercially in the SPALAX system. With the support of GCMC simulations and experimental modeling, we showed that xenon is adsorbed at the surface of silver nanoparticles in the zeolite [15]. The amount of silver and the particle size (and conversely, the dispersion) are key parameters that directly determine the number of adsorption sites and thus the capacity of the adsorbent in the presence of a ppm-level concentration of xenon.

Active carbons will no doubt be replaced by silver-containing zeolites in the next generation of xenon air concentrator devices regardless of the type of zeolite (Ag-mordenite [17], Ag-ETS-10 [13], or Ag-chabazite). The instability of the nanometer-sized silver particles due to their tendency to migrate and aggregate irreversibly into larger nanoparticles is, however, a recurrent problem. The use of confining scaffolds, such as zeolite-type material, is often reported in the literature as an efficient solution to overcome particle migration at the surface and eventually grows, leading to a loss of performances [18,19]. Nevertheless, over the course of a pilot-scale study of the TSA process on site, we observed a drop in adsorption capacity that was concomitant with the appearance of AgCl and an apparent growth of silver nanoparticles at the zeolite surface.

The objectives of this study are (i) to determine why xenon adsorption capacity decreases, with a special focus on understanding the origin and role of Cl; (ii) to study regeneration parameters that can restore the adsorption capacity; and (iii) to validate the regeneration process in the context of a cyclic TSA process in relevant conditions. For this purpose, a careful, systematic parameter study has been carried out using fresh and Cl-contaminated Ag@ZSM-5 for quantitative comparison under representative static and dynamic conditions. Beyond this particular xenon separation application, we highlight here the possible role of Cl in the acceleration/enabling of silver migration and/or aggregation into larger particles.

2. Results and Discussion

2.1. Deactivation Mechanisms of Ag@ZSM-5 Zeolite

2.1.1. Loss of Adsorption Capacities

When used in SPALAX process conditions, after permeation membranes where the Xe concentration is approximately 5 ppm, the adsorption capacities of the Ag@ZSM-5 zeolite tend to decrease after several TSA cycles. At this xenon partial pressure, the work of Deliere et al. has shown that the adsorption capacities of Ag@ZSM-5 are directly linked to the dispersion of the silver

nanoparticles with a size distribution around 2 nm [20]. In that respect, the 5 ppm xenon partial pressure was chosen as a reference in this study for following the behavior of the silver nanoparticles and the capacity of the adsorbent.

Adsorption isotherms were carried out on Ag@ZSM-5 positioned after the permeation membrane, and the results were compared with the fresh Ag@ZSM-5 sample and Na-ZSM-5 (prior to exchange with silver). Figure 1 presents the log-scale adsorption capacities of the three samples at 5 ppm of xenon.

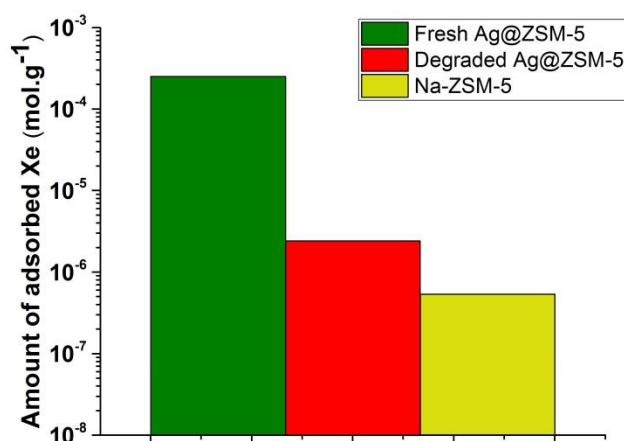


Figure 1. Xenon adsorption capacity at 5 ppm (298 K) for the fresh (green) and degraded (red) Ag@ZSM-5 and for Na-ZSM-5 (yellow). Y-scale in Log.

The “fresh” Ag@ZSM-5 provides the reference value for xenon adsorption for the present study: $2.5 \times 10^{-4} \text{ mol}\cdot\text{g}^{-1}$. In comparison, the degraded sample presents a xenon adsorption capacity of only $2.4 \times 10^{-6} \text{ mol}\cdot\text{g}^{-1}$, which corresponds to a loss of more than 99% of the initial xenon adsorption capacity. The capacity of this sample approaches that of Na-ZSM-5, which means that the adsorption property of the silver nanoparticles has essentially disappeared.

2.1.2. Identification of the AgCl Phase upon the Adsorption Step

In order to determine the origin of this loss of adsorption capacity, XRD measurements were performed on the fresh and degraded samples to determine whether structural changes have occurred (Figure 2).

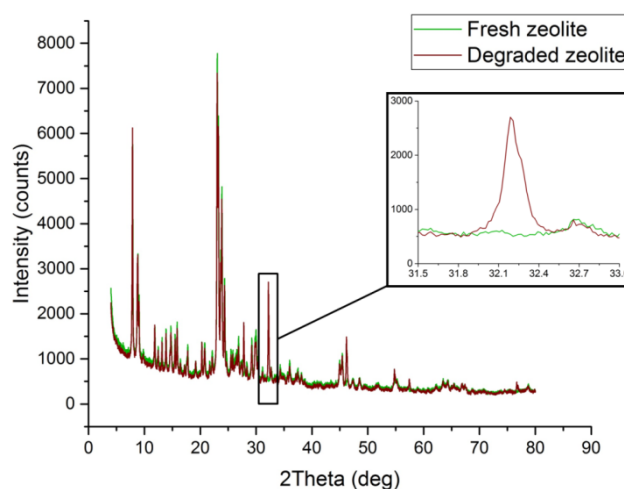


Figure 2. XRD patterns of fresh (green) and degraded (red) zeolite samples; (insert) zoom on the 31.5–33° range to highlight one peak of the AgCl Chlorargyrite CFC (PDF 85-1355).

At first glance, the XRD patterns are very similar for the two samples, corresponding mostly to ZSM-5 zeolite with additional silver FCC peaks at 38° , 46° , and 64° . For the degraded Ag@ZSM-5, however, additional peaks appear at 27.8° and 32.3° . These peaks correspond to the presence of a face-centered cubic AgCl phase (ICDD patterns ref: 00-031-1238). This clearly indicates the conversion of silver nanoparticles with chlorinated compounds present in the gas phase (outlet of the permeation membranes). This observation is confirmed by the XPS analysis with the apparition of an AgCl phase after contamination (Supporting Information Figure S1) and by the elemental analysis of chlorine in the samples presented in Table 1. While the Cl concentration is lower than the detection limit (5 ppm) in the fresh zeolite, it rises to reach 0.40 wt.% in the degraded sample.

Table 1. Elemental analyses of chlorine in fresh and degraded samples.

Sample	Cl
Fresh Ag@ZSM-5	<5 ppmw *
Degraded Ag@ZSM-5	0.40 wt.%

* detection limit (5 ppmw).

Based on the work of Deliere et al. (saturation of strong adsorption sites at around 10^{-1} kPa Xe), the silver nanoparticles can adsorb 5×10^{-4} mol_{Xe}/g_{Ag}, requiring approximately two silver atoms per xenon atom. Consequently, we can estimate that there is about 10^{-3} mol_{Ag}/g_{Ag} at the surface of the silver nanoparticles. This dispersion value is consistent with a theoretical size distribution of silver nanoparticles between 0 and 20 nm, as shown in Figure S2 (supporting information).

Considering silver and chlorine contents of 9 wt.% and 0.40 wt.%, respectively, the ratio corresponds to 1.2×10^{-3} mol_{Cl}/g_{Ag}. This amount is slightly higher than the amount of silver at the surface of the nanoparticles (10^{-3} mol_{Ag}/g_{Ag}), which means that (i) chlorine entirely covers the surface of the particles in a 1:1 stoichiometric amount, and (ii) the excess of Cl can form AgCl particles (bulk). Although it cannot be quantified, the formation of an AgCl phase is visible in XRD. In order to determine whether the formation of AgCl (whether at the surface or in the bulk) is at the origin of the drop in adsorption capacity, a molecular modeling study was carried out.

Simulations were performed to study and compare the adsorption capacities of 2-nm silver chloride nanoparticles with respect to pure silver nanoparticles.

2.1.3. Simulation of AgCl Nanoparticle Adsorption

The results of the molecular simulation of xenon adsorption on a 2-nm silver chloride nanoparticle are shown in Figure 3. We also report the results obtained with a silver nanoparticle of the same size (Deliere et al.) [15,20]. The adsorption of xenon on AgCl nanoparticles is extremely low and even negligible with respect to adsorption on silver nanoparticles. At 5×10^{-4} kPa (corresponding to 5 ppm Xe), the adsorption capacity on the silver nanoparticle is 1.2×10^{-3} mol_{Xe}/g_{Ag}, while it is 2.4×10^{-12} mol_{Xe}/g_{AgCl} for silver chloride. These simulations show qualitatively that xenon adsorption is much degraded by the presence of silver chloride at the surface of the nanoparticles. This is fully consistent with the experimental results reported in the present work. After contamination, Xe adsorption is probably performed mainly within the zeolite network and on the residual pure silver particles.

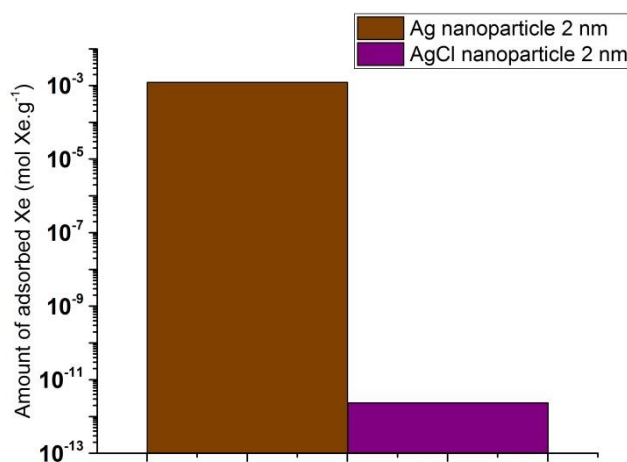


Figure 3. Simulation of the xenon adsorption capacity at 5 ppm (298 K) on silver (brown) and silver chloride (purple) nanoparticles. Plot is indicated in a log scale.

From a physical viewpoint, this drastic difference between silver and silver chloride particles can be explained by the change in the polarizability of the system. While Ag^0 has a very large polarizability (large number of electrons), both Ag^+ and Cl^- possess a much smaller polarizability (because Ag^+ is a cation and Cl^- has a much smaller number of electrons compared to Ag). As a result, because Xe interacts only through the dispersion interactions (with a constant linked to the polarizability of Xe and the atoms forming the nanoparticles), this drop in adsorption capacity between silver and silver chloride nanoparticles was expected. Xenon adsorption on AgCl nanoparticles is negligible, which explains the drop in adsorption performance at low xenon partial pressures. In this situation, the adsorption of xenon is achieved mainly by the zeolite network. Finally, the loss of xenon adsorption capacity can be explained by the loss of the available silver metal surface due to the formation of AgCl.

2.2. Identification of the Chlorine-Containing VOCs

We identified four chlorine-containing VOCs in the air processed by the permeation membrane, namely trichloromonofluoromethane, trichloroethane, tetrachloromethane, and tetrachloroethylene (see Figure S3 in supporting information). In order to elucidate whether these chlorine-containing organics could be at the origin of the surface poisoning and/or the formation of the AgCl phase, a series of sample collections before and after Ag@ZSM-5 zeolite were carried out and analyzed. For each experiment, the sample collection was performed at 30 NL h⁻¹ for 2 h on a Tenax tube at room temperature:

- Tenax T1 was placed directly behind the nitrogen membranes to identify the compounds in the gas flow.
- Tenax tube T2 was placed after a column containing 3 g of Ag@ZSM-5.
- Tenax tube T3 was placed after a column containing 3 g of Ag@ZSM-5, which was then eluted at 623 K with a nitrogen flow, in order to determine if the compounds are only physisorbed or if they react with the silver particles.

Figure S4 (supporting information) schematizes these experiments and the operating conditions. From the difference between the Tenax tubes, we can easily observe that the four organic chlorides are adsorbed onto the Ag@ZSM-5 and do not desorb even at 623 K. We can thus conclude that they all react with silver nanoparticles and should form strongly adsorbed species, which are likely chemically bonded, as well as an AgCl phase. At this stage, we cannot rule out the possibility that other Cl-VOCs, such as inorganic Cl-containing compounds (Cl_2 , HCl), may be present in the feed and may also react with the silver nanoparticles.

Based on these results, a synthetic gas containing 5 ppm of Xe, and 10 ppb each of 1,1,1-trichloroethane, tetrachloromethane, and tetrachloroethylene in nitrogen was prepared and used hereafter as a model contaminated feed to permit a reproducible aging study in representative conditions.

2.3. Regeneration Temperature of Ag@ZSM-5

In order to use the Ag@ZSM-5 in process conditions and to prevent the loss of adsorption capacity observed in the previous section, we studied different temperatures of regeneration over the course of the TSA process and desorption step.

2.3.1. Heat Treatment Effect

We assumed that a heat treatment at high temperature might degrade the adsorbent regardless of the presence or absence of Cl-VOCs. Before considering the regeneration of a degraded sample, the effect of a heat treatment alone on the Ag@ZSM-5 adsorption capacity was studied (in the absence of Cl-VOCs) (Figure 4).

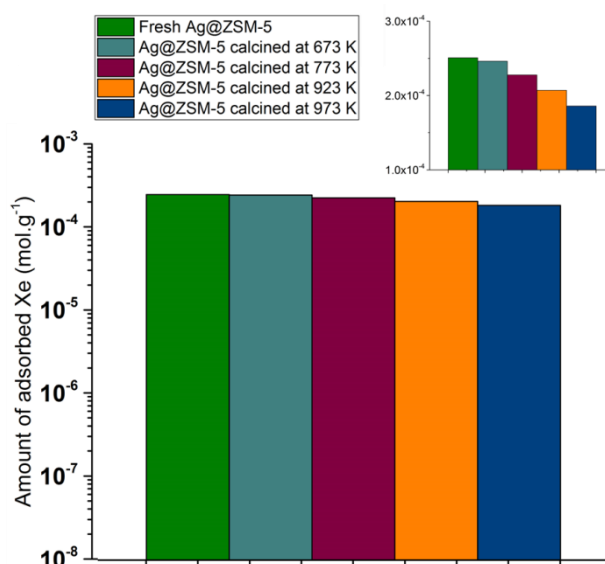


Figure 4. Xenon adsorption capacity at 5 ppm (298 K) on Ag@ZSM-5 calcined at several temperatures (from 623 K to 973 K). Y-axis in a log scale; (insert) zoom with linear scale.

Figure 4 highlights a slight but significant loss of adsorption capacity from 298 K (no heating) to 973 K. Indeed, for a xenon pressure of 5×10^{-4} kPa (corresponding to 5 ppm), the difference in adsorption capacity is equal to 25.6%, and only 1.4% between the fresh sample and the one calcined again at 673 K.

The melting point of silver is 1235 K [21], but we observe a change in adsorption performance for temperatures above 673 K. This agrees with the observations made by Tammann [22], which indicates that a solid-state compound becomes reactive when its temperature exceeds half of its melting temperature ($1235/2$ in K). Based on this conclusion, the main hypothesis is that heat energy enables silver nanoparticles to migrate and grow at temperatures above 673 K. Above this temperature, the active surface of the silver nanoparticles decreases by sintering, which explains this capacity loss. This sintering phenomenon could be due to Ostwald ripening and/or particle migration and coalescence [23,24]. While the migration of nanoparticles in the zeolite porous network can hardly be monitored, we can confirm a sintering phenomenon occurring at the surface of a zeolite crystal by means of STEM observations (Figure 5). Starting from room temperature with many small nanoparticles

at the surface, the silver sintered to form large particles at 623 K. This sintering phenomenon can be observed below 673 K.

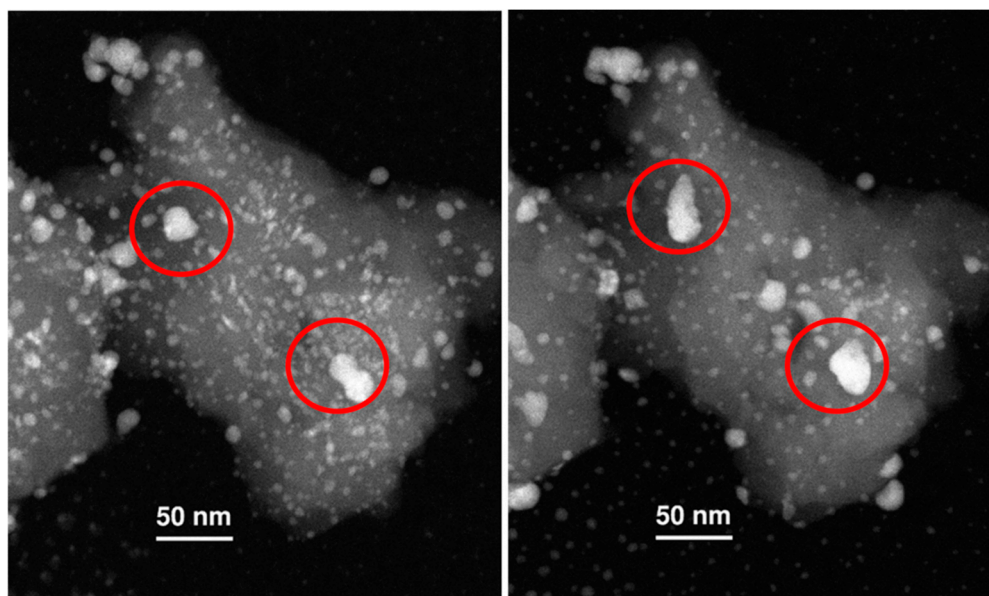


Figure 5. Scanning Transmission Electron Microscopy—High Angle Annular Dark Field (STEM-HAADF) images showing the sintering mechanism suffered by the fresh Ag@ZSM-5 sample under 1 mbar of N₂ with a 4 K/min temperature ramp from room temperature (**left**) to 623 K (**right**).

To limit silver nanoparticle migration and sintering, the temperature of 623 K was selected for the regeneration step.

2.3.2. Study of the Regeneration of Ag@ZSM-5 at 623 K

The degraded sample (by aging with the model CI-VOCs stream) presented in the previous section was heated under nitrogen at 623 K. The adsorption isotherms performed on this sample before and after the heat treatment are represented on Figure 6.

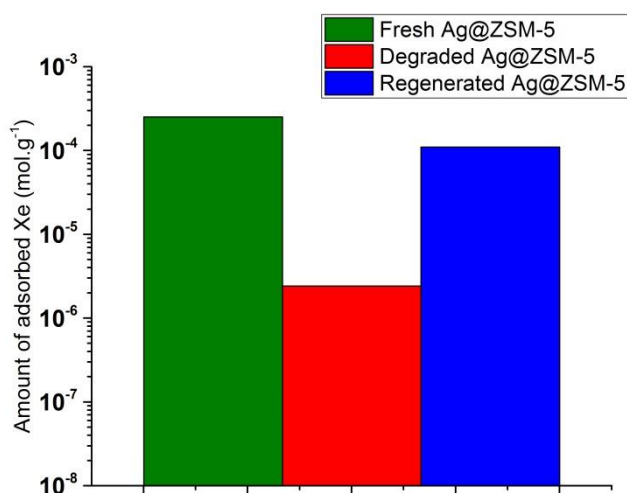


Figure 6. Xenon adsorption capacity at 5 ppm for the fresh (**green**), degraded (**red**), and regenerated (**blue**) Ag@ZSM-5. Plot is indicated in a log scale.

Starting from the degraded zeolite with a xenon adsorption capacity of $2.4 \times 10^{-6} \text{ mol}\cdot\text{g}^{-1}$, the heat treatment allowed the recovery of most of its capacity: $1.1 \times 10^{-4} \text{ mol}\cdot\text{g}^{-1}$. This regenerated sample is

close to the fresh zeolite with xenon capacities higher than 10^{-4} mol·g⁻¹. We assumed that the heat treatment under N₂ would evacuate most of the chloride and clean the surface of the nanoparticles. After the heat treatment under nitrogen at 623 K, the chloride content decreased from 0.40 wt.% to 62 ppmw (Table 2).

Table 2. Elemental analyses of chloride in fresh, degraded, and regenerated Ag@ZSM-5 samples.

Sample	Cl
Fresh Ag@ZSM-5	<5 ppmw
Degraded Ag@ZSM-5	0.40 wt.%
Regenerated Ag@ZSM-5	62 ppmw

The XRD analyses, represented in Figure 7, are consistent with this evacuation of chloride compounds upon the heat treatment under nitrogen. The peak at 32° that corresponds to AgCl is hardly visible.

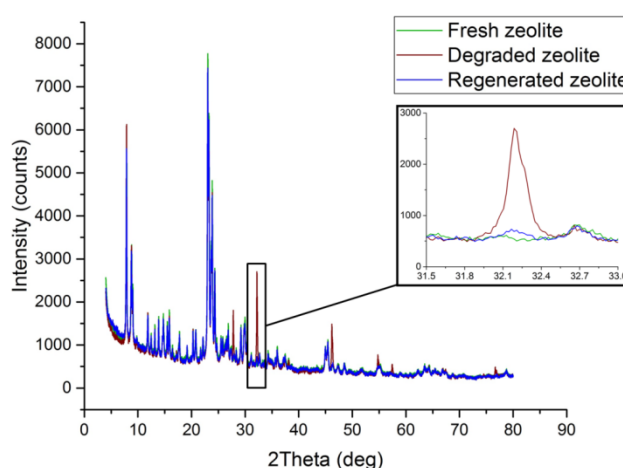


Figure 7. XRD patterns of fresh (green), degraded (red), and regenerated (blue) zeolite samples; (insert) zoom on the range 31.5–33° to highlight one peak of the AgCl Chlorargyrite CFC (PDF 85-1355).

Following the same logic as in Section 2.1.2, 62 ppm corresponds to 1.9×10^{-5} mol_{Cl}/g_{Ag} (with a silver content of 9 wt.% in Ag@ZSM-5), and is therefore very inferior to the amount of silver at the surface of the particles (1×10^{-3} mol_{Ag}/g_{Ag}). This result means that a considerable part of the active surface of the silver nanoparticles is available for xenon adsorption. Indeed, this amount of chloride is insufficient to cover the surface of all the silver nanoparticles: it can occupy only around 2% of the silver adsorption sites. As a first approximation, it is possible to consider that the presence of a chloride will disturb not only the silver atom with which it is linked, but also the four direct neighbors (Face Centered Cubic FCC network). Thus, considering that 10% ((4 + 1) × 2 %) of the silver sites are incapable of adsorbing xenon, this corresponds to an adsorption capacity of 2.3×10^{-4} mol·g⁻¹ (90% of the fresh zeolite adsorption capacity). This capacity being much higher than that obtained experimentally (1.1×10^{-4} mol·g⁻¹); this means either that the presence of a chloride disrupts much more than the four direct neighbors, or that another phenomenon such as sintering also explains the loss of capacities (or a combination thereof).

It is therefore possible to regenerate most of the xenon adsorption capacities by using a heat treatment under nitrogen flow. With a temperature of 623 K, there is still a slight amount of chloride in the zeolite that could be accumulated over a number of cycles, but a higher temperature would also reduce the performances by promoting sintering mechanisms.

2.4. Validation of Regeneration Process under TSA Cycles

The deactivation mechanisms and the identification of the chlorinated compounds responsible for this deactivation were verified using a bench test with breakthrough curves in a TSA cycling process.

The adsorption capacity equilibrium is determined for a given gas from the breakthrough curve by integrating the time-resolved signal until the time at which the gas mole fraction at the outlet reaches the inlet mole fraction. Different breakthrough curves are represented in Figure 8 to highlight the shift of the curves over the course of the cycles for the sample exposed to chlorinated compounds.

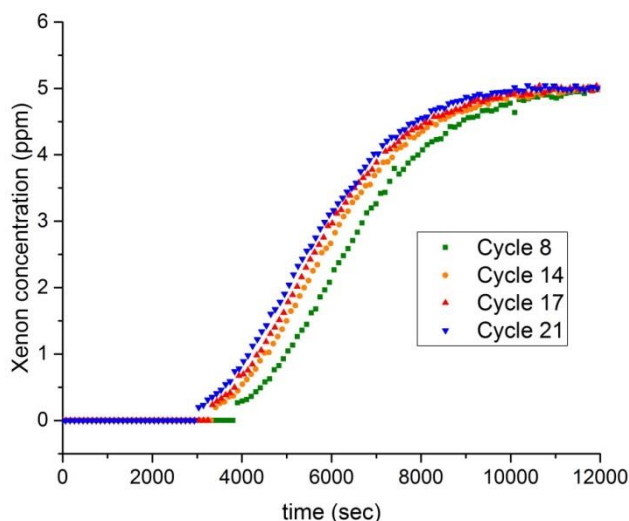


Figure 8. Breakthrough curves obtained at different cycles (room temperature) for a gas mixture containing 5 ppm of xenon in nitrogen with 10 ppb each of 1,1,1-trichloroethane, tetrachloromethane, and tetrachloroethylene. The flow rate is 80 mL/min, while the adsorbent mass is around 0.3 g.

For each breakthrough curve, the uncertainty was evaluated and corresponds to the usual propagation error law with the relevant parameters: the time resolution of the gas chromatography device and its measurement, the flow rate, the dead volumes, and the mass of adsorbent. The uncertainty bar was then slightly increased and fixed at 4%. The results of the two aging processes performed with or without the chlorinated compounds are presented in Figure 9.

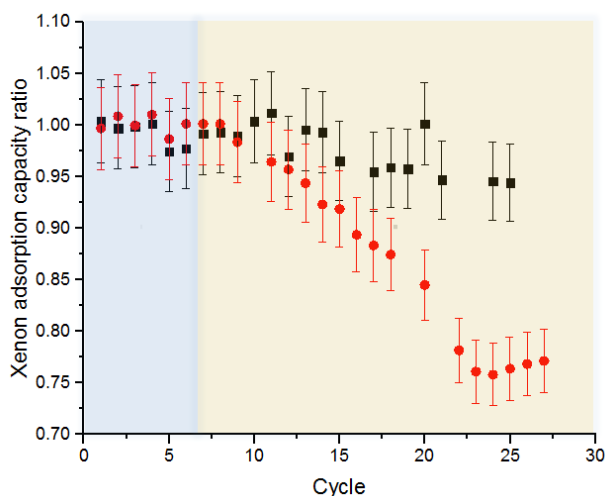


Figure 9. Aging of two Ag@ZSM-5 columns with and without chlorinated organic compounds. The blue background corresponds to the first phase with a contact time of 4 hours and a flow rate of 80 mL/min; the red background corresponds to a contact time of 19 h and a flow rate of 160 mL/min.

While the xenon adsorption capacities remain almost stable over the different cycles for the mixture containing only xenon and nitrogen, the performance of the zeolite decreases in the presence of chlorinated compounds. Initially, the chlorinated compounds were brought to contact only during the xenon breakthrough—which means a contact time of 4 hours at 80 mL/min. However, because the concentration of the chlorides was very low, their amount was insufficient to initiate a clear degradation. Moreover, the elemental analyses and the heat treatment impact show that a large proportion of the chlorinated compounds are evacuated upon each regeneration step. Starting from cycle 6, therefore, the flow rate and the duration were progressively increased (after the breakthrough) to reach a contact time of 19 h and a flow rate of 160 mL/min, and quickly the xenon adsorption capacities started to decrease. This experiment thus highlights the impact of the identified chlorinated compounds on the Ag@ZSM-5 zeolite. It seems that there is a mixture of two contributions: the reaction of gas with solid to produce an inactive phase (AgCl) and the sintering of silver nanoparticles promoted by the chlorinated compounds. These two contributions cannot be distinguished in this study, because regeneration at a high temperature is needed to perform a breakthrough experiment. It is possible to describe the degradation on the basis of the duration of contamination and the flow rate (amount of chlorinated compounds passed through the column) or the sintering with the number of regeneration steps. Moreover, even if the regeneration step makes it possible to reduce the amount of chlorine in the zeolite, part of the chlorine may be accumulated over the course of the cycles. This experiment can indeed be paralleled with the results of Sections 2.1 and 2.3: A slight accumulation of Cl, as revealed by elemental analyses, could be responsible for the decrease in xenon adsorption capacity.

All of these results suggest the following deactivation mechanism: During the contamination step, chloride compounds react with silver and form silver chloride according to a vapor-solid type reaction as described by Bartholomew [23]. Then, during the regeneration step, silver chloride is regenerated into silver. The regeneration enables the adsorbent to recover its performance in terms of xenon uptake, but a small amount of silver chloride is accumulated over the cycles and leads to a progressive deactivation of the silver nanoparticles. In addition to this vapor-solid reaction, a sintering effect promoted by the formation of AgCl could explain the coarsening observed. Indeed, with the melting point of silver chloride being lower than that of silver (728 K for AgCl versus 1235 K for silver), we can assume that the sintering of AgCl nanoparticles would be facilitated.

3. Materials and Methods

3.1. Sample Preparation

3.1.1. Adsorbent Synthesis

The Ag@ZSM-5 adsorbent was prepared according to the method previously described in Deliere et al. [15,20]. In brief, the preparation of Ag@ZSM-5 consisted of an ionic exchange between a suspension of Na-ZSM-5 zeolite (Tosoh ©, Tokyo, Japan; Si/Al = 14.5) and an aqueous solution of silver nitrate (Alfa Aesar ©, Ward Hill, MA, USA), followed by a drying step and a heat-treatment step under N₂ at 673 K for 4 hours in order to generate silver nanoparticles. The resulting Ag@ZSM-5 was pressed into pellets, ground, sieved to a 315–500 µm fraction, and used as such in the separation columns.

3.1.2. Degradation and Regeneration Steps

In order to study the influence of Cl-based contaminants present in the air, two samples were aged in the column using different gas mixtures and temperature conditions, and were then compared with a fresh sample.

- The “fresh sample” corresponds to the Ag@ZSM-5 zeolite after heat treatment at 673 K in N₂ as reported above.
- The “degraded sample” corresponds to Ag@ZSM-5 exposed to Cl-containing VOCs. The degradation protocol consists in feeding a column of fresh zeolite with a Cl-VOC concentrated

stream. In order to concentrate the airstream with relevant VOCs encountered in the SPALAX system, atmospheric air was treated by six nitrogen generator membranes (UBE N₂ Separator, UBE©, Tokyo, Japan) [25]. The degradation protocol was applied for a column filled with 13 g of fresh Ag@ZSM-5 at room temperature under a flow of air treated by membranes at 300 NL·h⁻¹ for 168 h.

- The “regenerated sample” corresponds to the degraded sample mentioned above, which is then regenerated in a column by means of heat treatment in N₂. The regeneration gas was nitrogen (BIP grade, Air Products©, Allentown, PA, USA) under a flow of 200 NL·h⁻¹ for 48 h. After a study of the temperature effect (detailed below), the temperature chosen for the validation using a cyclic TSA process was 573 K.

The specific times used for degradation (168 h) and regeneration (48 h) have been chosen so as to wean off the effects of kinetics. These times have not been optimized but are long enough to provide enough chlorinated compounds or to evacuate them respectively.

3.1.3. Heat Treatments

Starting from a fresh sample of Ag@ZSM-5, various samples were prepared by inflicting an additional heat treatment for 6 hours, in order to study the influence of temperature regeneration on this adsorbent. After the heat treatment at 673 K for the preparation of the adsorbent, Ag@ZSM-5 was heated again from room temperature to a set temperature at 15 K min⁻¹ and then kept hot for 6 hours in a tubular oven under N₂ atmosphere (BIP grade, Air Products ©, Allentown, PA, USA). The tubular oven was then cooled to room temperature. This study was carried out at four different temperatures: 673, 773, 923, and 973 K.

3.2. Experimental Techniques

3.2.1. Isothermal Adsorption Experiments

Xenon isotherms were performed using a Belsorp-Max apparatus (Bel, Tokyo, Japan) with 5.0 grade xenon (Nexeco Air, Leersum, Netherlands). This apparatus is a Sievert-type system that is equipped with three staged pressure sensors (0.1 Torr, 10 Torr, and 1000 Torr) to measure the pressure down to 6×10^{-3} Pa, which corresponds to 0.06 ppm. The temperature was regulated by a thermal bath at 298 K. The typical sample mass was around 0.4 g. Prior to adsorption measurements, the samples were outgassed under vacuum: 10⁻² kPa at 623 K for 4 hours, and then 10⁻⁵ kPa at 623 K for 16 h. The set-up parameters used for the adsorption isotherm measurements (including equilibrium conditions) can be found in Daniel et al. [14]. The adsorption equilibrium was assumed to be reached when the pressure variation was less than 0.3% after 300 s.

3.2.2. XRD Analyses

X-ray diffraction (XRD) powder patterns were recorded at 2θ between 5 and 80° with Cu Kα1 (λ = 1.5406 Å), using a D8 Advance A25 device (Bruker ©, Billerica, MA, USA). They were used to identify the crystalline structure of the nanoparticles [26].

3.2.3. XPS Analyses

In order to confirm the observation of the XRD analysis, the fresh and degraded samples were characterized with x-ray photoelectron spectroscopy (XPS). A monochromatic, Al Kα (1486.6 eV) x-ray source was used in the XPS measurements (15 kV × 15 mA = 225 W) using an AXIS ULTRA DLD (Kratos Analytical ©, New York, NY, USA).

3.2.4. Elemental Analyses

Chlorine was quantified by subjecting samples prepared in a Schöniger flask to an ionic chromatography analysis (experimental uncertainty $\pm 5\%$). The silver loading was measured by ICP-OES (inductively coupled plasma optical emission spectrometry; uncertainty $\pm 3\%$). The results of the elemental analyses are given in mass units.

In order to identify and quantify the concentration of organochlorine compounds in the air used herein, air samples were adsorbed in Tenax concentrator tubes. The compounds were then detected with a quadrupole mass spectrometer upon thermal desorption.

3.2.5. STEM Analyses

The HAADF-STEM observations (environmental mode) were performed on an FEI TITAN environmental microscope (ETEM 80–300 keV) equipped with a spherical aberration corrector for the objective lens. In order to analyze the samples in relevant conditions, each sample was placed in the microscope, and then the temperature was increased from room temperature to 623 K with a ramp of 4 K/min while maintaining a constant pressure of 1 mbar of N_2 .

3.3. Bench Test for Aging of Ag@ZSM-5

To verify the influence of the chlorinated VOCs identified in the air on the aging of Ag@ZSM-5, dynamic chromatographic separations, hereinafter referred to as breakthroughs, were performed. The experimental set-up used in the present work to obtain breakthrough curves for Xe is illustrated in Figure S5 (supporting information). The breakthrough curves were carried out at ambient temperature in a column (6.28 mm internal diameter \times 50 mm height) containing about 0.3 g of adsorbent. Three gases were used for this test: nitrogen (BIP grade, Air Products©, Allentown, PA, USA) for the regeneration step; a mixture of 5 ppm of xenon in nitrogen (blank); and a bottle of 5 ppm of xenon in nitrogen with 10 ppb each of 1,1,1-trichloroethane, tetrachloromethane, and tetrachloroethylene (both prepared by Air Products ©).

First, the column was activated with N_2 at 573 K for 2 hours and cooled at 300 K for 1 hour. Then the gas mixtures containing xenon (with or without the presence of Cl-VOCs) were used at 300 K to perform the breakthrough until the saturation zone was reached (around four hours). Initially, the column was closed after the breakthrough until the next cycle, but then, in order to accelerate the deactivation phenomenon with chlorinated compounds, the duration and flow rate of gas circulation after the breakthrough were modified (from zero to 15 h, and from 80 mL/min to 160 mL/min). In order to unravel the origin of the decay in capacity over the course of the cycles, the same process conditions were applied in parallel on two columns of Ag@ZSM-5. Twenty-five breakthroughs with a xenon-in-nitrogen mixture were performed on the first column, while 27 breakthroughs were performed on the second column with a mixture of xenon and chlorinated organic compounds in nitrogen. For the regeneration and breakthrough steps, the gas mixtures were passed through the column at a flow rate of 80 mL/min. The xenon concentrations at the column outlet were determined by using gas chromatography coupled with a thermal conductivity detector (VARIAN, 490-GC).

3.4. Molecular Simulation

In order to compare the adsorption of xenon on silver nanoparticles and silver chloride nanoparticles, molecular simulation—namely the Grand Canonical Monte Carlo method—was performed following the same conditions as those presented in Deliere et al. [15,20].

3.4.1. Preparation of AgCl Nanoparticles for Simulation

First, silver chloride nanoparticles were built from a large face-centered cubic (FCC) structure of crystalline silver chloride with a lattice parameter equal to 5.622 Å. Silver chloride nanoparticles with a

diameter of 2, 3, 4, and 5 nm were simulated, and each one was placed in a cubic simulation box at least twice as large as the nanoparticle. The nanoparticles were then thermally relaxed at 500 K.

3.4.2. Grand Canonical Monte Carlo Simulations

Xenon adsorption was simulated by means of Monte Carlo simulations in the Grand Canonical ensemble (GCMC). This stochastic method simulates a system with a constant volume V in equilibrium with an infinite reservoir of gas molecules—Xe in this case—imposing its temperature and chemical potential (so that the gas pressure is also imposed). The Lennard-Jones potentials used to model the interaction between the xenon atoms and the atoms of the silver chloride nanoparticles are gathered in Table 3. While some coefficients were found in the literature, the others were obtained using the Lorentz combination rules from like-atom parameters. Xenon adsorption on the silver chloride nanoparticles was studied in the pressure range from 10^{-6} to 100 kPa and compared with the results obtained by Deliere et al. for silver nanoparticles [15].

Table 3. Lennard-Jones parameters used in this work ^a.

		σ (Å)	ϵ (K)	Ref
Ag ⁺	Ag ⁺	2.186	54.34519	LB
Cl ⁻	Cl ⁻	3.934	419.3958	LB
H ₂ O (SPCE)	H ₂ O (SPCE)	3.166	78.17659	[27]
Xe	Xe	3.849	281	[28]
Ag ⁺	H ₂ O (SPCE)	2.676	65.18068	[29]
Cl ⁻	H ₂ O (SPCE)	3.55	181.0716	[29]
Ag ⁺	Xe	3.0175	123.5759	LB
Cl ⁻	H ₂ O (SPCE)	3.8915	343.2932	LB

^a LB indicates that the Lennard-Jones parameters were obtained using the Lorentz-Berthelot combining rules.

4. Conclusions

We studied the effects of temperature and the presence of chloride compounds on the xenon adsorption capacity of Ag@ZSM-5. It was shown that some chlorides present in the air react with the silver Ag⁰ nanoparticles at room temperature (vapor-solid reaction), which deactivates the strong adsorption sites (silver nanoparticles) and favors their sintering during the regeneration phase at 573–623 K. This study has shown by experimental and simulation methods that the formation of a silver chloride phase is critical for xenon adsorption, and a priori for noble gases more generally. Regarding the effect of the temperature, the isotherms show that there is no critical loss of adsorption capacity below 973 K, but the performances slightly decrease due to crystallite growth via a sintering mechanism. This result inspired a heat treatment study in the aim of recovering the xenon adsorption capacities of the material. This work revealed that a regeneration temperature at 623 K under nitrogen is able to evacuate most of the chlorides, but a small part is still accumulated over the course of the cycles. Finally, the use of a cyclic TSA process in the presence or absence of Cl-containing compounds demonstrated a slow loss of xenon adsorption capacities. It seems that there is a mixture of two contributions: the reaction of gas with solid to produce an inactive phase (AgCl) and the sintering of silver nanoparticles promoted by the chlorinated compounds.

Since Ag@ZSM-5 is a very promising material for xenon adsorption, this study could help to develop a process that would decrease the production cost of this rare gas and in turn encourage its more widespread use. The results of this study may also be relevant to any silver-doped material, whether zeolite-supported or not, since the reactive phase in our case is composed of nanoparticles. Thus, important catalytic reactions such as epoxidation [30] or DeNO_x [31] that use this kind of material may encounter similar complications, since air is involved in these processes.

A detailed study on silver particle migration and sintering fostered by Cl will be published elsewhere [32,33].

Supplementary Materials: The following are available online at <http://www.mdpi.com/2073-4344/9/8/686/s1>. Figure S1: X-ray photoelectron (XPS) measurement results recorded for the fresh (A) and degraded (B) Ag@ZSM-5 samples. While peak 1 and 2 correspond to silver, peak 3 and 4 are characteristic of an AgCl phase, Figure S2: Amount of silver (mol) at the surface of the nanoparticles per gram of silver and according to the particle size, Figure S3: Analysis at the membrane gas outlet of the organic chlorinated compounds. Gas analysis screening consisting of the adsorption of compounds for 2 h onto Tenax tube followed by thermodesorption and gas chromatography coupled to mass spectrometry, Figure S4: Schematic representation of the Tenax tubes preparation for the identification of Cl-COV in the process gas, Figure S5: Schematic representation of the breakthrough experiments on adsorptive materials. (a) The column (50 mm long \times 6 mm inner diameter) used for the breakthrough experiments is filled with the adsorbent (Ag@ZSM-5) and plugged with cotton and a steel mesh at each end. The steel tube is shown in grey while the steel mesh is in darker grey, the cotton in white and the adsorbent in speckled orange. (b) The experimental set-up is composed of the adsorption column as the central element positioned in a chromatographic oven used to precisely control the temperature during the breakthrough experiments. The gas is injected at a given pressure (air liquid valve) and flow (Bronkhorst controller El Flow: 80 mL/min) in the column by the head and exits at the bottom. The flow is then sent towards the gas chromatograph (VARIAN, 490-GC). This device is connected to a computer for signal acquisition and processing.

Author Contributions: All authors contributed to the preparation of the manuscript. The final version of the manuscript was approved by all authors. Conceptualization, A.M., G.C. and L.D.; Validation, S.T., B.C. and D.F.; Investigation, A.M., A.A., C.G., G.C. and B.C.; Resources, V.T., G.C., L.R. and L.C.; Writing—review and editing, A.M. and D.F.; Supervision, D.F.; Project administration, A.M., S.T. and D.F.

Funding: This research received no external funding.

Conflicts of Interest: The authors declare no conflict of interest.

References

1. Dubasov, Y.V.; Popov, Y.S.; Prelovskii, V.V.; Donets, A.Y.; Kazarinov, N.M.; Mishurinskii, V.V.; Popov, V.Y.; Rykov, Y.M.; Skirda, N.V. The APIKC-01 Automatic Facility for Measuring Concentrations of Radioactive Xenon Isotopes in the Atmosphere. *Instrum. Exp. Tech.* **2005**, *48*, 373–379. [[CrossRef](#)]
2. Cullen, S.C.; Gross, E.G. The Anesthetic Properties of Xenon in Animals and Human Beings, with Additional Observations on Krypton. *Science* **1951**, *113*, 580–582. [[CrossRef](#)] [[PubMed](#)]
3. Fraissard, J.; Ito, T. ^{129}Xe n.m.r. study of adsorbed xenon: A new method for studying zeolites and metal-zeolites. *Zeolites* **1988**, *8*, 350–361. [[CrossRef](#)]
4. Le Petit, G.; Douysset, G.; Ducros, G.; Gross, P.; Achim, P.; Monfort, M.; Raymond, P.; Pontillon, Y.; Jutier, C.; Blanchard, X.; et al. Analysis of Radionuclide Releases from the Fukushima Dai-Ichi Nuclear Power Plant Accident Part I. *Pure Appl. Geophys.* **2014**, *171*, 629–644. [[CrossRef](#)]
5. Achim, P.; Monfort, M.; Le Petit, G.; Gross, P.; Douysset, G.; Taffary, T.; Blanchard, X.; Moulin, C. Analysis of Radionuclide Releases from the Fukushima Dai-ichi Nuclear Power Plant Accident Part II. *Pure Appl. Geophys.* **2014**, *171*, 645–667. [[CrossRef](#)]
6. Topin, S.; Greau, C.; Deliere, L.; Hovesepian, A.; Taffary, T.; Le Petit, G.; Douysset, G.; Moulin, C. SPALAX new generation: New process design for a more efficient xenon production system for the CTBT noble gas network. *J. Environ. Radioact.* **2015**, *149*, 43–50. [[CrossRef](#)] [[PubMed](#)]
7. Le Petit, G.; Cagniant, A.; Gross, P.; Douysset, G.; Topin, S.; Fontaine, J.P.; Taffary, T.; Moulin, C. SpalaxTM new generation: A sensitive and selective noble gas system for nuclear explosion monitoring. *Appl. Radiat. Isot.* **2015**, *103*, 102–114. [[CrossRef](#)] [[PubMed](#)]
8. Crawford, P.G. Zeolite Membranes for the Separation of Krypton and Xenon from Spent Nuclear Fuel Reprocessing Off-Gas. Ph.D. Thesis, Georgia Institute of Technology, Atlanta, GA, USA, 2013.
9. Häussinger, P.; Glatthaar, R.; Rhode, W.; Kick, H.; Benkmann, C.; Weber, J.; Wunschel, H.-J.; Stenke, V.; Leicht, E.; Stenger, H. Noble Gases. In *Ullmann's Encyclopedia of Industrial Chemistry*; Wiley-VCH Verlag GmbH & Co. KGaA: Weinheim, Germany, 2000; ISBN 978-3-527-30673-2.
10. Kerry, F.G. *Industrial Gas Handbook: Gas Separation and Purification*; CRC Press: Boca Raton, FL, USA, 2007; ISBN 978-1-4200-0826-5.

11. Fontaine, J.P.; Pointurier, F.; Blanchard, X.; Taffary, T. Atmospheric xenon radioactive isotope monitoring. *J. Environ. Radioact.* **2004**, *72*, 129–135. [CrossRef]
12. Munakata, K.; Kanjo, S.; Yamatsuki, S.; Koga, A.; Ianovski, D. Adsorption of Noble Gases on Silver-mordenite. *J. Nucl. Sci. Technol.* **2003**, *40*, 695–697. [CrossRef]
13. Kuznicki, S.M.; Ansón, A.; Koenig, A.; Kuznicki, T.M.; Hastrup, T.; Eyring, E.M.; Hunter, D. Xenon Adsorption on Modified ETS-10. *J. Phys. Chem. C* **2007**, *111*, 1560–1562. [CrossRef]
14. Daniel, C.; Elbaraoui, A.; Aguado, S.; Springuel-Huet, M.A.; Nossov, A.; Fontaine, J.P.; Topin, S.; Taffary, T.; Deliere, L.; Schuurman, Y.; et al. Xenon Capture on Silver-Loaded Zeolites: Characterization of Very Strong Adsorption Sites. *J. Phys. Chem. C* **2013**, *117*, 15122–15129. [CrossRef]
15. Deliere, L.; Topin, S.; Coasne, B.; Fontaine, J.P.; De Vito, S.; Den Auwer, C.; Solari, P.L.; Daniel, C.; Schuurman, Y.; Farrusseng, D. Role of Silver Nanoparticles in Enhanced Xenon Adsorption Using Silver-Loaded Zeolites. *J. Phys. Chem. C* **2014**, *118*, 25032–25040. [CrossRef]
16. Monpezat, A.; Topin, S.; Deliere, L.; Farrusseng, D.; Coasne, B. Evaluation Methods of Adsorbents for Air Purification and Gas Separation at Low Concentration: Case Studies on Xenon and Krypton. *Ind. Eng. Chem. Res.* **2019**, *58*, 4560–4571. [CrossRef]
17. Munakata, K.; Fukumatsu, T.; Yamatsuki, S.; Tanaka, K.; Nishikawa, M. Adsorption Equilibria of Krypton, Xenon, Nitrogen and Their Mixtures on Molecular Sieve 5A and Activated Charcoal. *J. Nucl. Sci. Technol.* **1999**, *36*, 818–829. [CrossRef]
18. El-Roz, M.; Telegeiev, I.; Mordvinova, N.E.; Lebedev, O.I.; Barrier, N.; Behilil, A.; Zaarour, M.; Lakiss, L.; Valtchev, V. Uniform Generation of Sub-Nanometer Silver Clusters in Zeolite Cages Exhibiting High Photocatalytic Activity under Visible Light. *ACS Appl. Mater. Interfaces* **2018**, *10*, 28702–28708. [CrossRef]
19. Severance, M.; Dutta, P.K. Evolution of Silver Nanoparticles within an Aqueous Dispersion of Nanosized Zeolite Y: Mechanism and Applications. Available online: <https://pubs.acs.org/doi/abs/10.1021/jp5074957> (accessed on 23 April 2019).
20. Deliere, L. Adsorption et Séparation des Gaz Rares sur des Adsorbants Dopés à L'argent. Ph.D. Thesis, Université Claude Bernard–Lyon, Lyon, France, 2015.
21. Johnstone, A.H. *CRC Handbook of Chemistry and Physics*, 69th ed.; Chief, R.C., Weast, C.R.C., Eds.; CRC Press Inc.: Boca Raton, FL, USA, 1988; p. 2400, ISBN 0-8493-0369-5. *J. Chem. Technol. Biotechnol.* **1991**, *50*, 294–295. [CrossRef]
22. Tammann, G. *Lehrbuch der Metallkunde*, 4th ed.; Verlag Voss: Berlin, Germany, 1929.
23. Bartholomew, C.H. Mechanisms of catalyst deactivation. *Appl. Catal. A Gen.* **2001**, *212*, 17–60. [CrossRef]
24. Hansen, T.W.; DeLaRiva, A.T.; Challa, S.R.; Datye, A.K. Sintering of Catalytic Nanoparticles: Particle Migration or Ostwald Ripening. *Acc. Chem. Res.* **2013**, *46*, 1720–1730. [CrossRef]
25. Koros, W.J.; Paul, D.R. *Current Aspects of Membranes-Based Separation of Gases*; Chenoweth, M.B., Ed.; Hardwood Academic Publishers: New York, NY, USA, 1984; Volume 5.
26. Scherrer, P. Bestimmung der Größe und der inneren Struktur von Kolloidteilchen mittels Röntgenstrahlen. *Nachr. Von Der Ges. der Wiss. Zu Göttingen Math. Phys. Kl.* **1918**, *2*, 98–100.
27. Berendsen, H.J.C.; Grigera, J.R.; Straatsma, T.P. The missing term in effective pair potentials. *J. Phys. Chem.* **1987**, *91*, 6269–6271. [CrossRef]
28. Pellenq, R.J.M.; Nicholson, D. Grand Ensemble Monte Carlo Simulation of Simple Molecules Adsorbed in Silicalite-1 Zeolite. *Langmuir* **1995**, *11*, 1626–1635. [CrossRef]
29. Zarzycki, P.; Kerisit, S.; Rosso, K.M. Molecular Dynamics Study of the Electrical Double Layer at Silver Chloride–Electrolyte Interfaces. *J. Phys. Chem. C* **2010**, *114*, 8905–8916. [CrossRef]
30. Cheng, L.; Yin, C.; Mehmood, F.; Liu, B.; Greeley, J.; Lee, S.; Lee, B.; Seifert, S.; Winans, R.E.; Teschner, D.; et al. Reaction Mechanism for Direct Propylene Epoxidation by Alumina-Supported Silver Aggregates: The Role of the Particle/Support Interface. *ACS Catal.* **2014**, *4*, 32–39. [CrossRef]
31. Liu, Z.; Ihl Woo, S. Recent Advances in Catalytic DeNOX Science and Technology. *Catal. Rev.* **2006**, *48*, 43–89. [CrossRef]

32. Ouyang, R.; Liu, J.-X.; Li, W.-X. Atomistic Theory of Ostwald Ripening and Disintegration of Supported Metal Particles under Reaction Conditions. Available online: <https://pubs.acs.org/doi/abs/10.1021/ja3087054> (accessed on 11 March 2019).
33. Bartholomew, C.H.; Farrauto, R.J. Catalyst Deactivation: Causes, Mechanisms, and Treatment. In *Fundamentals of Industrial Catalytic Processes*; John Wiley & Sons, Inc.: Hoboken, NJ, USA, 2005; pp. 260–336, ISBN 978-0-471-73007-1.



© 2019 by the authors. Licensee MDPI, Basel, Switzerland. This article is an open access article distributed under the terms and conditions of the Creative Commons Attribution (CC BY) license (<http://creativecommons.org/licenses/by/4.0/>).